

# Characteristic density contrasts in the evolution of superclusters. The case of A2142 supercluster (Research Note)

Mirt Gramann<sup>1</sup>, Maret Einasto<sup>1</sup>, Pekka Heinämäki<sup>2</sup>, Pekka Teerikorpi<sup>2</sup>, Enn Saar<sup>1,3</sup>, Pasi Nurmi<sup>2</sup>, and Jaan Einasto<sup>1,3,4</sup>

<sup>1</sup> Tartu Observatory, Observatooriumi 1, 61602 Tõravere, Estonia

<sup>2</sup> Tuorla Observatory, University of Turku, Väisäläntie 20, Piikkiö, Finland

<sup>3</sup> Estonian Academy of Sciences, Kohtu 6, 10130 Tallinn, Estonia

<sup>4</sup> ICRANet, Piazza della Repubblica 10, 65122 Pescara, Italy

Received / Accepted

## ABSTRACT

**Context.** The formation and evolution of the cosmic web in which galaxy superclusters are the largest relatively isolated objects is governed by a gravitational attraction of dark matter and antigravity of dark energy (cosmological constant).

**Aims.** We study the characteristic density contrasts in the spherical collapse model for several epochs in the supercluster evolution and their dynamical state.

**Methods.** We analysed the density contrasts for the turnaround, future collapse, and zero gravity in different  $\Lambda$ CDM models and applied them to study the dynamical state of the supercluster A2142 with an almost spherical main body, making it a suitable test object to apply a model that assumes sphericity.

**Results.** We present characteristic density contrasts in the spherical collapse model for different cosmological parameters. The analysis of the supercluster A2142 shows that its high-density core has already started to collapse. The zero-gravity line outlines the outer region of the main body of the supercluster. In the course of future evolution, the supercluster may split into several collapsing systems.

**Conclusions.** The various density contrasts presented in our study and applied to the supercluster A2142 offer a promising way to characterise the dynamical state and expected future evolution of galaxy superclusters.

**Key words.** large-scale structure of the Universe; galaxies: groups: general

## 1. Introduction

One of the most remarkable achievements of contemporary cosmology is the discovery of the cosmic web, which is a complex hierarchical network of galaxy systems in which galaxies, galaxy groups, clusters, and superclusters form interconnected systems separated by voids of various sizes (Jõeveer et al. 1977; Jõeveer & Einasto 1978; Zeldovich et al. 1982). In the cosmic web, the largest relatively isolated systems are galaxy superclusters (de Vaucouleurs 1956; Abell 1958; Jõeveer et al. 1978; Zucca et al. 1993; Einasto et al. 1994).

The evolution and dynamical state of superclusters have been analysed with several methods. One of them is the spherical collapse model. This model describes the evolution of a spherically symmetric perturbation in an expanding universe. Under the assumption of sphericity, the dynamics of a collapsing shell is determined by the mass in its interior. The spherical collapse model has been discussed in detail by Tolman (1934); Bondi (1947); Gunn & Gott (1972); Peebles (1980). This model has been used in the Press-Schechter formalism to evaluate the mass function of clusters (Press & Schechter 1974) and to analyse the infall of nearby galaxies into the Virgo cluster (e.g. Karachentsev et al. 2014). A spherical collapse model has been applied to study, for example, the Corona Borealis supercluster (Small et al. 1998; Pearson et al. 2014), the Shapley superclus-

ter (Reisenegger et al. 2000; Proust et al. 2006), and the A2199 supercluster (Rines et al. 2002).

One essential moment in the evolution of a spherical perturbation is called turnaround, the moment when the sphere stops expanding together with the universe and the collapse begins. At the turnaround, the perturbation decouples entirely from the Hubble flow of the homogeneous background. Gramann & Suhhonenko (2002) studied the dynamical state of superclusters in different  $\Lambda$ CDM models and showed that only a small fraction of superclusters or their high-density cores have already reached the turnaround radius and have started to collapse at the present epoch. Unlike clusters, superclusters have not reached a quasi-equilibrium configuration.

In the universe with a critical mass density all regions with overdensity would eventually collapse. In the standard  $\Lambda$ CDM model, the universe makes the transition from a matter-dominated to a dark-energy dominated stage at the redshift  $z \approx 0.3$ . As long as the matter density was substantially larger than the dark energy density, it dominated the evolution of the universe, decelerating the expansion and driving the formation of structures with gravitational instability. When the average matter density fell below two times the dark energy density (at the redshift  $z \approx 0.7$ ), the dark energy started accelerating the expansion, and the formation of structure slowed down. At the present epoch, when the acceleration of the expansion has recently started, the largest bound structures are just form-

ing. In the future evolution of the universe, these bound systems separate from each other at an accelerating rate, forming isolated “island universes” (Busha et al. 2005; Dünner et al. 2006; Araya-Melo et al. 2009). Dünner et al. (2006) analysed the spherical collapse model to find the minimum mass density required for a spherical shell to remain bound until a very distant future in an accelerating universe. This density criterion can be used to identify the superclusters that will eventually turnaround and collapse in the future. Luparello et al. (2011) used this approach to construct catalogues of superclusters from the SDSS data, and Chon et al. (2013, 2014) applied a similar concept to define X-ray superclusters. The mass density required for the future collapse is smaller than the density required for the turnaround and collapse at the present epoch.

The presence of the dark energy along with gravitating matter influences the formation of the large-scale structure at all scales from groups of galaxies to superclusters. Chernin (2001) introduced a zero-gravity scale, which describes the relation between the gravity force and the antigravity force due to dark energy. At the zero-gravity distance, gravity is equal to antigravity. This defines the minimum mass density for a gravitationally bound system at the present epoch (see also Teerikorpi et al. 2015, and references therein).

The aim of this *Research Note* is to analyse the different characteristic densities in the evolution of superclusters applying the spherical collapse model. We study the densities for the turnaround, future collapse, and for zero gravity in different  $\Lambda$ CDM models (Sect. 2). We apply our results to the galaxy supercluster A2142 (Einasto et al. 2015, hereafter E2015) in Sect. 3. The A2142 supercluster has a close to spherical high-density main body. This makes it a suitable object to apply methods, which assume sphericity for the study of its dynamical state.

We use the Hubble parameter  $H_0 = 100 h \text{ km s}^{-1} \text{ Mpc}^{-1}$ .

## 2. Characteristic density contrasts

The density perturbation in the volume  $V$  can be calculated as

$$\Delta\rho = \rho/\rho_m, \quad (1)$$

where  $\rho = M/V$  is the matter density in the volume and  $\rho_m = \Omega_m \rho_{\text{crit}} = 3\Omega_m H_0^2/8\pi G$  is the mean matter density in the local universe. For a spherical volume  $V = 4\pi R^3/3$  one can find that

$$\Delta\rho = 0.86 \times 10^{-12} \Omega_m^{-1} \left( \frac{M}{h^{-1} M_\odot} \right) \left( \frac{R}{h^{-1} \text{ Mpc}} \right)^{-3}. \quad (2)$$

From Eq. (2) we can estimate the mass of a structure as

$$M(R) = 1.16 \times 10^{12} \Omega_m \Delta\rho (R/h^{-1} \text{ Mpc})^3 h^{-1} M_\odot. \quad (3)$$

Table 1 summarises the characteristic density contrasts in different  $\Lambda$ CDM models for  $\Omega_m$  values  $\Omega_m = 0.3, 0.27$ , and  $1.0$ . The value  $0.3$  is suggested by the Planck results ( $\Omega_m = 0.308 \pm 0.012$ , Planck Collaboration et al. 2015),  $\Omega_m = 0.27$  was used in E2015 in the study of the A2142 supercluster (below), and  $\Omega_m = 1$  is used for heuristic reasons (see also Martínez & Saar 2002). Table 1 shows the density contrast  $\rho/\rho_m$  and also the density contrasts  $\rho/\rho_\Lambda$ , where  $\rho_\Lambda = \Lambda/8\pi G = \Omega_\Lambda \rho_{\text{crit}}$  is the density in the local universe, which corresponds to the cosmological constant (dark energy), and  $\rho/\rho_{\text{crit}}$ . We consider the flat cosmological models, where  $\Omega_\Lambda = 1 - \Omega_m$ .

### 2.1. Turnaround

The spherically averaged radial velocity around a system in the shell of radius  $R$  can be written as  $u = HR - v_{\text{pec}}$ , where  $v_H = HR$  is the Hubble expansion velocity and  $v_{\text{pec}}$  is the averaged radial peculiar velocity towards the centre of the system. At the turnaround point, the peculiar velocity  $v_{\text{pec}} = HR$  and  $u = 0$ . If  $v_{\text{pec}} < HR$ , the system expands, and if  $v_{\text{pec}} > HR$ , the system begins to collapse.

In the spherical collapse model, the peculiar velocity  $v_{\text{pec}}$  is directly related to the density contrast  $\Delta\rho$ . If  $\Delta\rho > \Delta\rho_T$ , then the perturbed region ceases to expand and begins to collapse. For  $\Omega_m = 1$ , the density fluctuation at the turnaround point is  $\Delta\rho_T = (3\pi/4)^2 = 5.55$  (see also Martínez & Saar 2002). The values of the turnaround parameters for various cosmological models were given in Chon et al. (2015).

For  $\Omega_m = 0.27$  and  $\Omega_\Lambda = 0.73$  the density perturbation at the turnaround point is  $\Delta\rho_T = 13.1$ . In this case, the mass of a structure at the turnaround point is

$$M_T(R) = 4.1 \times 10^{12} (R/h^{-1} \text{ Mpc})^3 h^{-1} M_\odot. \quad (4)$$

The mass  $M_T(R)$  describes the minimum mass needed in the sphere with radius  $R$  for the turnaround and collapse (Gramann & Suhhonenko 2002). For the same value of  $\Omega_m$ , the turnaround density in the open model is somewhat higher than in the flat model (see e.g. Regos & Geller 1989; Gramann & Suhhonenko 2002). However, the effect of the dark energy on  $\Delta\rho_T$  is small.

### 2.2. Future collapse

Dünner et al. (2006) studied the spherical collapse in the flat  $\Lambda$ CDM model with  $\Omega_m = 0.3$  ( $\Delta\rho_T = 12.2$ , see Table 1). They found that the minimum density required for a shell to remain bound in this model is  $\rho = 7.86 \rho_m$  (2.36 times the critical density  $\rho_{\text{crit}}$ ). All systems where the matter density is  $\rho = (7.86 - 12.2) \rho_m$  continue to expand at a decelerating rate and eventually turnaround and collapse in the future. At the present epoch, the minimum density for a shell to remain bound is  $\rho = 7.86 \rho_m = 3.37 \rho_\Lambda$ . At the final state, when this shell will turnaround and collapse, the density in the shell is  $\rho_f = 2 \rho_\Lambda$  (Dünner et al. 2006).

The density criterion  $\rho > 7.86 \rho_m$  was used by Araya-Melo et al. (2009) to identify the superclusters in the numerical simulations. They analysed the future evolution of these kinds of superclusters from the present time to an expansion factor  $a = 100$ . The spatial distribution of the superclusters remained essentially the same after the present epoch, reflecting the halting growth of the cosmic web as the dark energy starts to dominate. During evolution, the superclusters become more spherical and clusters in superclusters may merge into one cluster.

Density contrasts for the future collapse for different cosmological models were studied by Chon et al. (2015), who showed that for  $\Omega_m = 0.27$  the density contrast  $\Delta\rho_{\text{FC}} = 8.73$ . In this case, the minimum mass of the structure that will turnaround and collapse in the future is

$$M_{\text{FC}}(R) = 2.7 \times 10^{12} (R/h^{-1} \text{ Mpc})^3 h^{-1} M_\odot. \quad (5)$$

The future evolution of superclusters depends on the properties of the dark energy. For the same value of  $\Omega_m$ , the density contrast for the future collapse in the open model can be substantially smaller than that in the flat model (see e.g. Chon et al.

2015). In these models the growth of the structure also slows down when the curvature starts to dominate, but this process is not as rapid as in the models with the dark energy. In the open model with  $\Omega_m = 0.3$ , the  $\Delta\rho_{FC} = 2.87$  only.

### 2.3. Zero gravity

We can write the force affecting a test particle with mass  $m$  as the sum of Newton's gravity force produced by the mass  $M$  and Einstein's antigravity force due to the dark energy (Chernin et al. 2009),

$$F(R) = \left( -\frac{GM}{R^2} + \frac{8\pi G}{3}\rho_\Lambda R \right) m = \frac{4\pi}{3} GR (-\rho + 2\rho_\Lambda) m. \quad (6)$$

The gravity and antigravity are equal if  $\rho = 2\rho_\Lambda$  (density contrast  $\rho/\rho_m = 2\Omega_\Lambda/\Omega_m$ ). In this case, the acceleration around the system in the shell of radius  $R$  is  $du/dt = 0$ . If  $\rho < 2\rho_\Lambda$ , the system expands with an accelerating rate ( $du/dt > 0$ ). This criterion can be used to define the minimum mass density for a gravitationally bound system at the present epoch (Chernin et al. 2012; Teerikorpi et al. 2015). For the flat model with  $\Omega_m = 0.27$ , we find that the density contrast  $\Delta\rho_{ZG} = 5.41$ . In this case, the mass of the structure is

$$M_{ZG}(R) = 1.7 \times 10^{12} (R/h^{-1} \text{ Mpc})^3 h^{-1} M_\odot. \quad (7)$$

If the mass of the system is smaller than  $M_{ZG}(R)$  then the system is not gravitationally bound.

In the standard  $\Lambda$ CDM model, the mass density required for the future collapse is higher than the mass density for a gravitationally bound system at the present epoch. Not all gravitationally bound systems remain bound in the future. During evolution systems with  $\rho = (5.41 - 8.73)\rho_m$  continue to expand along with the universe. At the final state, when the shells with  $\rho_f = 2\rho_\Lambda$  turnaround, the zero-gravity scale coincides with the turnaround scale.

Table 1 presents the characteristic density contrasts for the turnaround, future collapse, and zero gravity. For comparison, we also calculated the characteristic density contrasts for the virialised systems. The virial densities were calculated using the approximation derived by Bryan & Norman (1998).

We also show the characteristic density contrasts for the linear mass scale in Table 1. In this case, the matter density is equal to the mean matter density and  $\Delta\rho = 1$ . The radial velocity around a system reaches the Hubble velocity  $u = HR$  ( $v_{pec} = 0$ ). This linear scale is also called the Einstein-Straus radius (Einstein & Straus 1945; Teerikorpi et al. 2015). From Eq. (3) we find that the linear mass of the structure, which corresponds to the mean density for  $\Omega_m = 0.27$ , is

$$M_L(R) = 0.3 \times 10^{12} (R/h^{-1} \text{ Mpc})^3 h^{-1} M_\odot. \quad (8)$$

For the underdense regions, the mass of the structure  $M(R) < M_L(R)$ .

## 3. Application to the A2142 supercluster

We apply the methods described above to study the dynamical state of the A2142 supercluster. It is the supercluster SC1 001 at the redshift  $z \approx 0.09$  from Liivamägi et al. (2012) supercluster catalogue in which superclusters of galaxies were determined on the basis of the luminosity density field of the Sloan Digital Sky Survey (SDSS) MAIN sample galaxies. Liivamägi et al. (2012) showed that in the supercluster SC1 001 the luminosity density

**Table 1.** Characteristic density contrasts.

	(1)	(2)	(3)	(4)
	$\Omega_m$	$\rho/\rho_m$	$\rho/\rho_\Lambda$	$\rho/\rho_{crit}$
Virial				
1.0	178	-	178	
0.3	340	146	102	
0.27	360	133	97	
Turn-around				
1.0	5.55	-	5.55	
0.3	12.2	5.21	3.65	
0.27	13.1	4.85	3.54	
Future collapse				
0.3	7.86	3.37	2.36	
0.27	8.73	3.23	2.36	
Zero gravity				
0.3	4.67	2.0	1.40	
0.27	5.41	2.0	1.46	
Linear				
0.3	1.0	0.43	0.3	
0.27	1.0	0.37	0.27	

**Notes.** See Sect. 2 for column explanations.

(calculated with  $8 h^{-1}$  Mpc smoothing length,  $D8$ ) is the highest in the whole SDSS MAIN survey region. Recently, E2015 presented a detailed study of this supercluster proposing to call it the A2142 supercluster, according to its richest galaxy cluster A2142. Details about the supercluster can be found in E2015. In accordance with E2015 we use the following standard cosmological parameters below: the matter density  $\Omega_m = 0.27$  and the dark energy density  $\Omega_\Lambda = 0.73$  (Komatsu et al. 2011).

The morphology of this and other superclusters from Liivamägi et al. (2012) catalogue was studied in Einasto et al. (2011a) who showed that the A2142 supercluster consists of a quite spherical main body with outgoing straight filament-like tail. This makes the A2142 supercluster, and especially its main body, a suitable test object to apply methods that assume sphericity.

E2015 analysed the luminosity density distribution in the A2142 supercluster and showed that it can be divided into four global density regions. Two high-density regions form a high-density core of the supercluster, lower density regions form the outskirts of the supercluster. Figure 1 presents the sky distribution of galaxies in these global luminosity density regions, and Table 2 summarises their properties.

The A2142 supercluster with its outgoing filament is quite asymmetrical, therefore we apply a spherical collapse model to the main body of the supercluster, and to the two group regions in the tail of the supercluster, as explained below. In addition to regions defined on the basis of the luminosity density, we choose the main body of the supercluster as follows: we use luminosity density limit  $D8 = 5$  (this is the luminosity density limit used to define superclusters in Liivamägi et al. 2012), and exclude two regions with galaxy groups from the tail of the superclusters, denoted as (2) and (3) in Fig. 1. These two regions are analysed separately (see E2015 for details about these regions). In addition, we study the local environment of the main body of the supercluster denoted as Main+env in Table 2. This region has no strict density limit. The radii of the regions are given in Table 2. Table 2 shows that, in addition to the main body of the supercluster, the "Main+env" region only includes the close neigh-

bourhood of its main body, approximately  $2 h^{-1}$  Mpc from the supercluster boundaries. This is underdense region penetrated by filaments of galaxy groups and single galaxies outgoing from the supercluster. These outgoing filaments were shortly discussed in E2015.

Masses of different global density regions are calculated as follows. Data about galaxy groups in the A2142 supercluster were taken from the group catalogue by Tempel et al. (2014), who also calculated group masses on the basis of the virial theorem. We summed group masses in each region, which gives the dynamical mass of the region. We also calculated the estimated masses. In each region there are some single galaxies. They may be the brightest galaxies of faint groups in which other member galaxies are too faint to be observed within SDSS survey magnitude limits. We used the median mass of groups with less than five member galaxies in the supercluster as the mass of these faint groups. To obtain the total mass of these faint groups, this median mass was multiplied with the number of single galaxies in a region. In addition, we added 10% of the total mass to the mass of the region as the mass of intracluster gas. The details and references of the calculations of dynamical and estimated masses can be found in E2015. The supercluster's total estimated mass is approximately 1.5 times larger than its dynamical mass. This agrees quite well with the estimates given in Chon et al. (2014), who compared supercluster masses from observations and simulations. In Table 2, we give the density contrasts of these global density regions calculated using dynamical and estimated masses and radii of these regions.

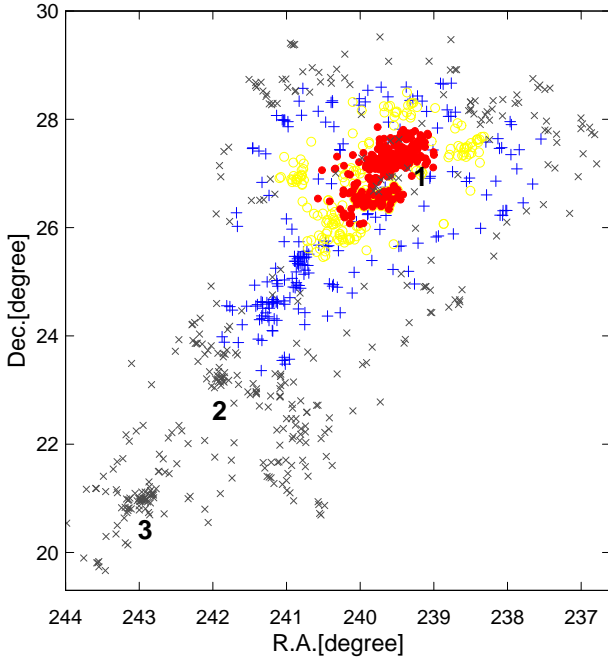


**Fig. 1.** Distribution of galaxies in the A2142 supercluster in the sky plane in global density regions as described in the text. Red filled circles denote galaxies in the region of global density  $D8 \geq 17$ ; yellow empty circles correspond to galaxies with global density  $13 \leq D8 < 17$ . Blue crosses correspond to galaxies with global density  $8 \leq D8 < 13$ , and grey Xs galaxies with  $5 \leq D8 < 8$ . The size of the highest density region is approximately 1.8 degrees, and the size of the region with  $D8 \geq 13$  is approximately 3 degrees; sizes in megaparsecs are given in Table 2. Number 1 marks the Abell cluster A2142, and numbers 2 and 3 indicate two regions of galaxy groups in the tail of the supercluster, as explained in the text.

**Table 2.** Density contrasts, masses, and radii of the core and the outskirts regions of the A2142 supercluster.

(1)	(2)	(3)	(4)	(5)	(6)
$D8$	$M_{\text{dyn}}$	$M_{\text{est}}$	$R$	$\Delta\rho_{\text{dyn}}$	$\Delta\rho_{\text{est}}$
	$[10^{15}h^{-1}M_{\odot}]$	$[10^{15}h^{-1}M_{\odot}]$			
Full scl	2.9	4.3			
$\geq 17$	1.2	1.4	6	17.9	20.9
$\geq 13$	1.7	2.1	8	10.5	13.0
$\geq 8$	2.2	3.0	10	7.1	9.7
Main ( $\geq 5$ )	2.5	3.7	13	3.6	5.3
Main+env	2.8	4.6	15	2.6	3.2
(2)	0.10	0.18	2.5	20.4	36.7
(3)	0.30	0.42	2.5	61.2	85.7

**Notes.** Columns are as follows: (1): Global luminosity density  $D8$  of the regions (in units of mean luminosity density,  $\ell_{\text{mean}} = 1.65 \cdot 10^{-2} \frac{10^{10}h^{-2}L_{\odot}}{(h^{-1}\text{Mpc})^3}$ ). Main body of the supercluster is defined as  $D8 \geq 5$ , without group regions 2 and 3. Main+env denotes main body of the supercluster without group regions 2 and 3, but with local neighbourhood of the main body; see text for details); (2): the total dynamical mass of groups (in case of groups with 2 and 3 member galaxies we use median mass); (3): the total estimated mass of a region (including faint groups and intracluster gas, see text); (4): radius of the region (in  $h^{-1}$  Mpc); (5): density contrast of the region according to the dynamical mass; (6): density contrast of the region according to the estimated mass.

In Fig. 2 we plot mass  $M(R)$  versus radius of a sphere  $R$  for different characteristic density contrasts (Eq. (4), (5), (7), and (8)) and show both the dynamical and estimated masses of global density regions in the A2142 supercluster (in Fig. 2 Main+env region is denoted as "env").

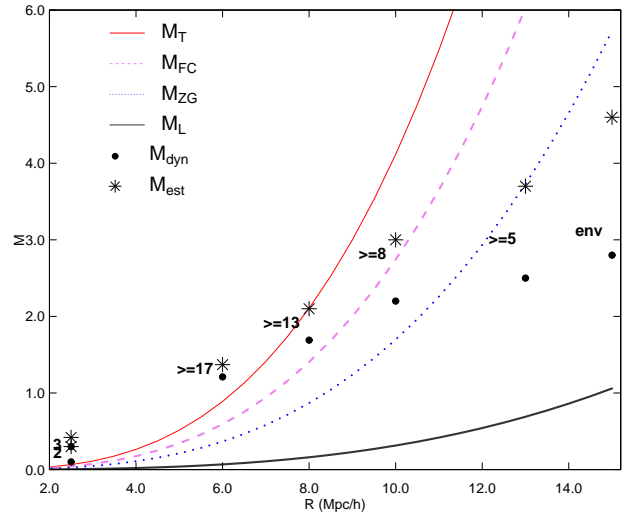


**Fig. 2.** Mass corresponding to the turnaround mass  $M_T(R)$  (red line), future collapse mass  $M_{\text{FC}}(R)$  (violet line), zero-gravity mass  $M_{\text{ZG}}(R)$  (blue line), and linear mass  $M_L(R)$  (grey line; in units of  $10^{15}h^{-1}M_{\odot}$ ) versus radius of a sphere  $R$  in different dynamical evolution models for  $\Omega_m = 0.27$ . Filled circles show the total masses of galaxy groups in regions of different global density in the A2142 supercluster (Table 2). Stars denote estimated masses as explained in the text. Numbers show global density lower limit for a region (env marks Main+env region, 2 and 3 denote regions of galaxy groups in the tail of the supercluster).

Figure 2 shows that points corresponding to the highest density core of the A2142 supercluster ( $D8 \geq 17$ ) lie well above the turnaround line, suggesting that this region has started to col-

lapse. The density contrasts of this region are high (Table 2). The cluster A2142 lies in this region. We note that most of the mass in this region comes from the mass of the cluster A2142 with dynamical mass  $M_{dyn} = 0.9 \times 10^{15} h^{-1} M_{\odot}$  in Tempel et al. (2014). This value is almost equal to the mass found by Munari et al. (2014) using several methods (see also discussion in E2015). Two group regions from the tail of the supercluster may have started to collapse, too.

According to the estimated mass, the full high-density core of the supercluster with  $D8 \geq 13$  may have reached the turnaround or is close to it. Lower global density regions do not have high enough mass for the present-day collapse. However, the estimated mass of the region with  $D8 \geq 8$  is high enough for this region to start the collapse in the future, as the FC line in Fig. 2 and the density contrast in Table 2 show. The outer parts of the supercluster with  $5 \leq D8 \leq 8$  may separate from the main body in the future. The filamentary tail of the supercluster (including group regions 2 and 3) lies below global density level  $D8 = 8$  and probably does not collapse in the future with supercluster main body. If we add this structure to the main body of the supercluster then the mass, as well as the volume, of the system increases. The increase in mass is not large enough for this system to collapse as a whole at present or in the future (Fig. 2). Taking into account that regions 2 and 3 collapse themselves, the most likely scenario is that these regions (or at least the region 3) will separate from supercluster's main body. Thus Fig. 2 suggests that the A2142 supercluster may split into several systems in the course of the future evolution.

According to the estimated mass, the gravity-antigravity balance line (zero gravity) in Fig. 2 borders the main body of the supercluster. Points corresponding to the region, which also includes the close environment of the supercluster lie below the zero gravity line suggesting that this region is not gravitationally bound. The linear mass scale lies farther away from the supercluster and its close neighbourhood. The zero-gravity line in Fig. 2 presents in another way some of the information given by the  $\Lambda$  significance graph ( $\log \rho/\rho_{\Lambda}$  vs.  $\log R$ ) introduced by Teerikorpi et al. (2015). This curve corresponds to the horizontal straight line  $\rho/\rho_{\Lambda} = 2$  in the  $\Lambda$  significance graph. The points lying above this line correspond to the high-density regions of the superclusters, as shown in the present paper for the A2142 supercluster.

## 4. Summary

We used the spherical collapse model to study the characteristic density contrasts in the evolution of superclusters. Despite its idealised nature, the spherical collapse model has been popular because of its simplicity. Also, this model gives a reasonable description of the collapse of high peaks in a random Gaussian density field (see e.g. Bernardeau 1994; Mo et al. 2010, and references therein).

We analysed the density contrasts for the turnaround, future collapse, and zero gravity in the  $\Lambda$ CDM models. The turnaround marks the epoch when the peculiar velocity reaches the Hubble velocity ( $v_{pec} = HR$ ) and the radial velocity around the system is  $u = 0$ . The mass density for the future collapse shows the density required for the perturbed region to continue to expand with an decelerating rate and eventually turnaround and collapse in the future. The zero gravity marks the epoch when the radial acceleration around the system is  $du/dt = 0$ : after that the perturbed region starts to expand with an accelerating rate.

Typically, rich superclusters have a complicated structure and the models which assume sphericity can be applied to their

central parts only (see e.g. Einasto et al. 2011a, for an analysis of supercluster morphology). The collapsing high-density cores have been studied in the very rich Shapley and Corona Borealis superclusters (Reisenegger et al. 2000; Pearson et al. 2014), in the Perseus-Pisces supercluster (Hanski et al. 2001; Teerikorpi et al. 2015), in the A2199 supercluster, the member of the Hercules supercluster (Rines et al. 2002; Einasto et al. 2001), and also in the richest supercluster of the Sloan Great Wall (Einasto et al. 2007, 2011b, and Heinämäki et al., in preparation). Chon et al. (2015) analysed the Shapley supercluster with the future collapse model and concluded that only the central part of the Shapley supercluster will form a supercluster in the distant future.

We applied our results to study the dynamical state of the supercluster A2142 with an almost spherical main body. Our analysis showed that the high-density core of the A2142 supercluster has already started to collapse. This conclusion was reached also by E2015. In the course of future evolution the supercluster may split into several collapsing systems. Araya-Melo et al. (2009) showed that during the future evolution, groups and clusters in superclusters may merge. In the A2142 supercluster, merging groups have been observed in the cluster A2142 region (Eckert et al. 2014) and perhaps in the outskirts of the high-density core of the supercluster (Kawahara et al. 2011). In the A2142 supercluster, the zero-gravity line borders the main body of the supercluster. This supports the conclusion that the A2142 supercluster does not remain bound in the future, its outer parts and tail may separate from the main body of the supercluster. Also, the close neighbourhood of the supercluster is not bound to the supercluster and may continue to expand together with the universe.

Density contrasts analysed in our study can be used to study the dynamical state and future evolution of a large sample of galaxy superclusters. The study of the galaxy properties in dynamically different regions may provide interesting insight for the environmental studies of the galaxies in superclusters. We will continue the study of the dynamical state of galaxy superclusters from observations and simulations in a forthcoming paper.

## Acknowledgments

We thank the referee for comments and suggestions that helped to improve the paper. We are pleased to thank the SDSS Team for the publicly available data releases. Funding for the Sloan Digital Sky Survey (SDSS) and SDSS-II has been provided by the Alfred P. Sloan Foundation, the Participating Institutions, the National Science Foundation, the U.S. Department of Energy, the National Aeronautics and Space Administration, the Japanese Monbukagakusho, and the Max Planck Society, and the Higher Education Funding Council for England. The SDSS Web site is <http://www.sdss.org/>. The SDSS is managed by the Astrophysical Research Consortium (ARC) for the Participating Institutions. The Participating Institutions are the American Museum of Natural History, Astrophysical Institute Potsdam, University of Basel, University of Cambridge, Case Western Reserve University, The University of Chicago, Drexel University, Fermilab, the Institute for Advanced Study, the Japan Participation Group, Johns Hopkins University, the Joint Institute for Nuclear Astrophysics, the Kavli Institute for Particle Astrophysics and Cosmology, the Korean Scientist Group, the Chinese Academy of Sciences (LAMOST), Los Alamos National Laboratory, the Max-Planck-Institute for Astronomy (MPIA), the Max-Planck-Institute for Astrophysics (MPA), New

Mexico State University, Ohio State University, University of Pittsburgh, University of Portsmouth, Princeton University, the United States Naval Observatory, and the University of Washington.

The present study was supported by the ETAG projects IUT26-2 and IUT40-2, and by the European Structural Funds grant for the Centre of Excellence "Dark Matter in (Astro)particle Physics and Cosmology" TK120. This work has also been supported by ICRAnet through a professorship for Jaan Einasto.

## References

- Abell, G. O. 1958, *ApJS*, 3, 211
- Araya-Melo, P. A., Reisenegger, A., Meza, A., et al. 2009, *MNRAS*, 399, 97
- Bernardeau, F. 1994, *ApJ*, 427, 51
- Bondi, H. 1947, *MNRAS*, 107, 410
- Bryan, G. L. & Norman, M. L. 1998, *ApJ*, 495, 80
- Busha, M. T., Evrard, A. E., Adams, F. C., & Wechsler, R. H. 2005, *MNRAS*, 363, L11
- Chernin, A. D. 2001, *Physics Uspekhi*, 44, 1099
- Chernin, A. D., Teerikorpi, P., Valtonen, M. J., et al. 2009, *A&A*, 507, 1271
- Chernin, A. D., Teerikorpi, P., Valtonen, M. J., et al. 2012, *A&A*, 539, A4
- Chon, G., Böhringer, H., Collins, C. A., & Krause, M. 2014, *A&A*, 567, A144
- Chon, G., Böhringer, H., & Nowak, N. 2013, *MNRAS*, 429, 3272
- Chon, G., Böhringer, H., & Zaroubi, S. 2015, *A&A*, 575, L14
- de Vaucouleurs, G. 1956, *Vistas in Astronomy*, 2, 1584
- Dünner, R., Araya, P. A., Meza, A., & Reisenegger, A. 2006, *MNRAS*, 366, 803
- Eckert, D., Molendi, S., Owers, M., et al. 2014, *A&A*, 570, A119
- Einasto, M., Einasto, J., Tago, E., Dalton, G. B., & Andernach, H. 1994, *MNRAS*, 269, 301
- Einasto, M., Einasto, J., Tago, E., Müller, V., & Andernach, H. 2001, *AJ*, 122, 2222
- Einasto, M., Gramann, M., Saar, E., et al. 2015, *A&A*, 580, A69
- Einasto, M., Liivamägi, L. J., Tago, E., et al. 2011a, *A&A*, 532, A5
- Einasto, M., Liivamägi, L. J., Tempel, E., et al. 2011b, *ApJ*, 736, 51
- Einasto, M., Saar, E., Liivamägi, L. J., et al. 2007, *A&A*, 476, 697
- Einstein, A. & Straus, E. G. 1945, *Reviews of Modern Physics*, 17, 120
- Gramann, M. & Suhhonenko, I. 2002, *MNRAS*, 337, 1417
- Gunn, J. E. & Gott, III, J. R. 1972, *ApJ*, 176, 1
- Hanski, M. O., Theureau, G., Ekholm, T., & Teerikorpi, P. 2001, *A&A*, 378, 345
- Jõeveer, M. & Einasto, J. 1978, in *IAU Symposium*, Vol. 79, *Large Scale Structures in the Universe*, ed. M. S. Longair & J. Einasto, 241–250
- Jõeveer, M., Einasto, J., & Tago, E. 1978, *MNRAS*, 185, 357
- Jõeveer, M., Einasto, J., & Tago, M. 1977, *Tartu Astrofüüs. Obs. Preprint*, Nr. A-1, 45 p., 1, A1
- Karachentsev, I. D., Tully, R. B., Wu, P.-F., Shaya, E. J., & Dolphin, A. E. 2014, *ApJ*, 782, 4
- Kawahara, H., Yoshitake, H., Nishimichi, T., & Sousbie, T. 2011, *ApJL*, 727, L38
- Komatsu, E., Smith, K. M., Dunkley, J., et al. 2011, *ApJS*, 192, 18
- Liivamägi, L. J., Tempel, E., & Saar, E. 2012, *A&A*, 539, A80
- Luparello, H., Lares, M., Lambas, D. G., & Padilla, N. 2011, *MNRAS*, 415, 964
- Martínez, V. J. & Saar, E. 2002, *Statistics of the Galaxy Distribution* (Chapman & Hall/CRC, Boca Raton)
- Mo, H., van den Bosch, F. C., & White, S. 2010, *Galaxy Formation and Evolution* (Cambridge University Press)
- Munari, E., Biviano, A., & Mamon, G. A. 2014, *A&A*, 566, A68
- Pearson, D. W., Batiste, M., & Batuski, D. J. 2014, *MNRAS*, 441, 1601
- Peebles, P. J. E. 1980, *The large-scale structure of the universe* (Princeton University Press)
- Planck Collaboration, Ade, P. A. R., Aghanim, N., et al. 2015, *ArXiv e-print*: 1502.01589
- Press, W. H. & Schechter, P. 1974, *ApJ*, 187, 425
- Proust, D., Quintana, H., Carrasco, E. R., et al. 2006, *A&A*, 447, 133
- Regos, E. & Geller, M. J. 1989, *AJ*, 98, 755
- Reisenegger, A., Quintana, H., Carrasco, E. R., & Maze, J. 2000, *AJ*, 120, 523
- Rines, K., Geller, M. J., Diaferio, A., et al. 2002, *AJ*, 124, 1266
- Small, T. A., Ma, C.-P., Sargent, W. L. W., & Hamilton, D. 1998, *ApJ*, 492, 45
- Teerikorpi, P., Heinämäki, P., Nurmi, P., et al. 2015, *A&A*, 577, A144
- Tempel, E., Tamm, A., Gramann, M., et al. 2014, *A&A*, 566, A1
- Tolman, R. C. 1934, *Proceedings of the National Academy of Science*, 20, 169
- Zeldovich, I. B., Einasto, J., & Shandarin, S. F. 1982, *Nature*, 300, 407
- Zucca, E., Zamorani, G., Scaramella, R., & Vettolani, G. 1993, *ApJ*, 407, 470